Non-contact atomic-force microscopy and density-functionnal theory studies of the (2×2) reconstructions of the polar AlN(0001) surface

Florian Chaumeton,[1,2] Roberto Robles,[3,4] Miguel Pruneda,[3,4] Nicolás Lorente,[3,4,*]
Benoit Eydoux,[1,2] Xavier Bouju,[1] Sébastien Gauthier,[1] and David Martrou[1,†]

[1] *NanoSciences Group, CEMES, CNRS UPR 8011, 29 rue J. Marvig, F-31055 Toulouse, France*
[2] *Université de Toulouse, UPS, 29 rue J. Marvig, F-31055 Toulouse, France*
[3] *ICN2 – Institut Catala de Nanociencia i Nanotecnologia, Campus UAB, 08193 Bellaterra (Barcelona), Spain*
[4] *CSIC – Consejo Superior de Investigaciones Cientificas, ICN2 Building, Campus UAB, 08193 Bellaterra (Barcelona), Spain*

(Dated: September 30, 2016)

Combined experimental and theoretical studies permit us to determine new protocols for growing by molecular beam epitaxy the technologically interesting N-rich AlN surfaces. This is achieved by dosing the precursor gases at unusually low rates. With the help of calculated structures by using density functionnal theory and Boltzmann distribution of the reconstructed cells, we proposed to assign the measured surface obtained with a growth rate of 10 nm/h to a (2×2) reconstructed surface involving one additionnal N atom per unit cell. These N-rich AlN surfaces could open new routes to dope AlN layers with important implications in high-power and temperature technological applications.

PACS numbers: 68.35.bg, 68.35.Rh, 68.37.Ps, 81.05.Ea

High-power electronic devices require materials with large electron mobilities and densities and large band gaps. Group-III nitride semiconductors are ideal candidates for these applications [1]. Among these materials, aluminium nitride (AlN) has the largest band gap [2]. It also has unique properties such as small density, large stiffness, large piezoelectric constant [3], large fracture resistivity and chemical inertness [4]. Recently, the two-dimensional electron gases appearing at the interface of a strained GaN quantum well sandwiched between relaxed AlN layers have permitted the realization of field effect transistors with a high cut-off frequency of 104 GHz [5]. Unfortunately, defects and interface states seriously compromise devices based on these materials and there is an urgent need for high-quality interfaces and surfaces. For these reasons, its surface reconstructions have received a lot of attention theoretically [6–11]. Furthermore, due to its high ionicity, AlN crystallizes in the wurtzite structure and its (0001) growth surface is polar, like other zinc blende (001) semiconductor surfaces [12]. The consequence of this polarity is that the crystal should be stabilized by the formation of surface charges that can be generated by different mechanisms like surface reconstructions (see the review article by Noguera [13] and references therein).

Experimentally, due to the large gap of AlN (6.2 eV) it is not possible to observe its surface by scanning tunneling microscopy (STM) except for the Al rich phase as explored by Lee *et al.* [14]. One effective way to get information at the atomic scale is to use atomic-force microscopy in the non contact mode (NC-AFM), as developped by Albrecht *et al.* in 1991 [15]. NC-AFM allows the observation of surfaces with atomic resolution of some ionic [16–19] and metal oxide compounds [20–25]. It was also used to study semiconductor surfaces such as Si(111) [26], GaAs [27], InSb [28] and diamond C(100)-(2×1) [29]. All these substrates can be prepared by cleavage or ionic bombardment followed by a soft annealing. In the case of nitride semiconductors, the layers should be grown under ultra-high vacuum (UHV) and then transferred into an AFM chamber under UHV, since their surfaces are not stable in air. We were able to realize the NC-AFM study of AlN(0001) using a custom-made equipment [30] where the AlN layer is grown by molecular beam epitaxy (MBE) using ammonia (NH_3) as nitrogen precursor and transferred under UHV to a room temperature AFM. With the help of calculations based on density functional theory (DFT), coupled to the experimental RHEED and NC-AFM measurements acquired for two different growth conditions, we proposed to assign one of the obtained surfaces to a (2×2) reconstruction involving one additional N atom per unit cell, and the other to a mixing between two alternative reconstructions functionnalized by hydrogen.

In the following sections, we first recall the electrostatic stability condition for crystals with polar surfaces. Using Bader charge analysis of the electronic density calculated by DFT for three (2×2) reconstructions, we check that this condition is fulfilled. Finally we present the effects of the different parameters (temperature and partial pressures) on the expected type of reconstructions and we use these results to analyse our experimental *in situ* reflection high-energy electron diffraction (RHEED) and NC-AFM measurements.

AlN crystallizes in the wurtzite structure with cell parameters $a = 3.112$ Å and $c = 4.982$ Å at 300 K [31].

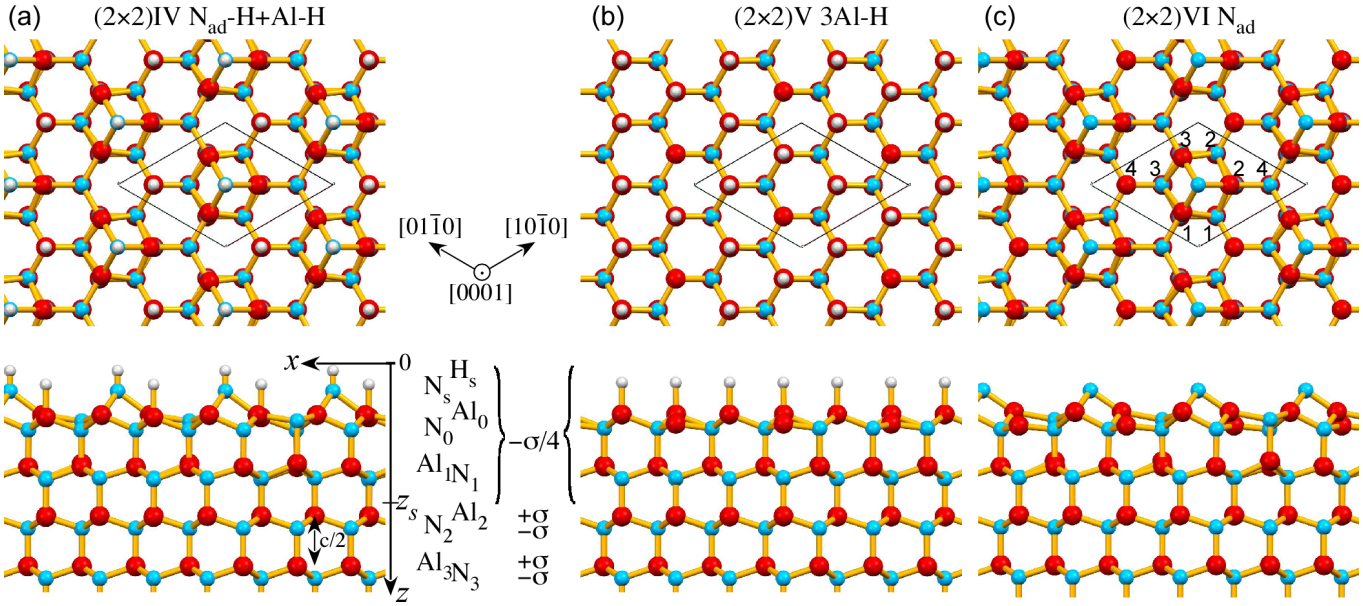

FIG. 1. Top and side views along the [1$\bar{1}$00] axis of the atomic models of the three (2×2) reconstructions, N_{ad}-H+Al-H, 3Al-H, and N_{ad} obtained by DFT. The (2×2) unit cell appears on the top views as a black lozenge. Al, N and H atoms are represented as red, blue and white balls respectively.

AlN(0001) layers can be described as a stacking of AlN bilayers distant by $c/2$ along the [0001] direction [Fig 1-(a)]. Each bilayer comprises an Al plane separated from a N plane by $c/8$. As AlN is a iono-covalent semiconductor, each atom carries a net charge of $+\delta$ for Al atoms and $-\delta$ for N atoms, leading to a macroscopic dipole moment pointing out of the (0001) surface. It is well-known that such a situation leads to the divergence of the electrostatic energy which is generally avoided by a modification of the surface layers of the sample [12, 13]. Goniakowski *et al.* have shown that this electrostatic divergence is removed when the following *electrostatic stability condition* is fulfilled [32]:

$$\sigma_S(z_S) = \frac{\mu_B(z_S)}{S\Delta z}\,, \qquad (1)$$

with $\sigma_S(z_S) = \int_0^{z_S} \mathrm{d}z\ \bar{\rho}(z)$, $\mu_B(z_S) = S\int_{z_S}^{z_S+\Delta z} \mathrm{d}z\ z\ \bar{\rho}(z)$, and $\bar{\rho}(z) = \frac{1}{S}\int \mathrm{d}x \int \mathrm{d}y\ \rho(x,y,z)$. (x,y,z) is defined such that the z axis is perpendicular to and pointing toward the surface [see Fig 1-(a)]. z_S defines the transition between the surface layer and the bulk, S is the area of the two-dimensional unit cell parallel to the surface, Δz is the crystal periodicity perpendicular to the surface. $\mu_B(z_S)$ is the dipole moment of the bulk unit cell along the z axis, $\bar{\rho}(z)$ is the lateral average of the total charge density $\rho(x,y,z)$, and $\sigma_S(z_S)$ is the surface charge density of the surface region defined by $0 < z < z_S$. The application of these equations to the wurtzite structure leads to $\sigma_S(z_S) = -\sigma/4$ where σ is the surface charge density of the top atomic plane of a bulk bilayer as defined in Fig. 1-(a). This can be checked for the particular case of AlN(0001): here $\mu_B(z_S) = 2\times(-\delta)\times c/8$, $\Delta z = c$ and $S = \sqrt{3}a^2/2$, leading to $\sigma_S(z_S) = -\sigma/4$ where $\sigma = \delta/S = 2\delta/\sqrt{3}a^2$ is the surface charge density of an Al plane.

Atom	1	2	3	4	σ_S
N_s	−2.201				−0.550
Al_0	2.322	2.322	2.322	2.348	
N_0	−2.386	−2.385	−2.385	−2.305	−0.587
Al_1	2.388	2.388	2.388	2.354	
N_1	−2.381	−2.381	−2.381	−2.405	−0.595
Al_2	2.387	2.387	2.387	2.386	
N_2	−2.387	−2.387	−2.387	−2.388	−0.595

TABLE I. Bader charges of Al and N atoms for the reconstruction VI(N_{ad}). The numerotation of atoms is indicated in Fig 1(c). σ_S is the surface charge density in $|e|/S$.

As shown in the next section, the three reconstructions that are accessible in our MBE growth conditions are the (2×2) reconstructions called IV(N_{ad}-H+Al-H), V(3Al-H), and VI(N_{ad}). Additionally, the atomic structures obtained from DFT calculations are presented in Fig 1 [33]. Here, we focus on the VI(N_{ad}) which corresponds to our experimental observations. This reconstruction has an additional N atom (N_s) linked to three Al atoms of the surface plane Al_0 [see Fig 1(c)]. Table I shows the Bader charges [34] for the Al and N atoms of the VI(N_{ad}) reconstruction. The positions of the atoms labelled 1 to 4 are indicated in Fig 1(c) for the two kinds of bilayer. Due to the symmetry of the reconstruction, the Bader charges of the atoms labelled 1 to 3 are identical while it is slightly different for the fourth

atom. From the third bilayer, the Bader charges retrieve their bulk value, which is 2.388 ± 0.001 $|e|$ per Al atom. Therefore, the *electrostatic stability condition* states that $\sigma_S = -0.597$ $|e|/S$.

The additional N_s atom on the surface has a Bader charge of -2.2 $|e|$ leading to a surface charge density of -0.550 $|e|/S$, that is 8 % larger than the value given by the *electrostatic stability condition*. Adding the first AlN bilayer leads to a value of -0.587 $|e|/S$ and decreases the difference to 1.5 %. Finally, with the second AlN bilayer, the surface charge density is equal to -0.595 $|e|/S$ showing a very good agreement with the theoretical prediction. This behavior is also observable for the two other reconstructions N_{ad}-H+Al-H and 3Al-H [33]. This calculation confirms that the crystal is stabilized by its surface reconstructions. It also shows that an analysis based on partial atomic charges such as Bader charges is efficient to recover the electrostatic stability condition.

By combining total energy calculations based on DFT with thermodynamical considerations we can predict the surface reconstruction under given experimental conditions [35]. DFT calculations are performed using the VASP code [36–38], with plane wave basis set expanded with a cutoff of 500 eV using PAW potentials [39]. The PBE exchange and correlation functional is used thanks to its superiority to predict surface geometries [40]. The back side of the slab is passivated by pseudo-hydrogen atoms with a 0.75 $|e|$ charge [41, 42]. Our results confirm quantitatively those obtained by Akiyama *et al.* [10], with only very small differences originating from a different parameter set in the DFT codes [33]. The stability of these three reconstructions depends on the substrate temperature $T_{\text{substrate}}$ and on the partial pressures p_{Al} and p_{NH_3}. The modification from partial pressures into chemical potentials is performed by using the partition function of a molecular gas with its different degrees of freedom [33, 43]. We will use these calculations to determine which reconstructions are observed experimentally.

The growth of AlN samples was carried out in a MBE chamber equipped with a RHEED gun working at 15 keV. The AlN layer is grown on a 4H-SiC(0001) substrate following a recipe described elsewhere [33, 44]. Two kinds of samples were considered with growth speeds of 100 nm/h and 10 nm/h, corresponding to a measured beam equivalent pressure (BEP) for Al of 3×10^{-8} and 3×10^{-9} Torr respectively. After the growth under NH_3 at 2×10^{-6} Torr of a layer with a thickness of several 10 nm to 100 nm, the samples are cooled down under NH_3 with a pressure of 5×10^{-7} Torr until 800°C, and then the NH_3 exposition is interrupted allowing to reach a base pressure of 10^{-9} Torr when the substrate is at 300°C. All the obtained surfaces were characterized by NC-AFM, using a commercial room-temperature (RT) ultrahigh vacuum STM/AFM (Omicron NanoTechnology GmbH, Taunusstein, Germany). Silicon cantilevers provided by NanoSensors (PPP-QNCHR, Neuchâtel, Switzerland) were used, with no special preparation except a moderate heating (150°C) in vacuum.

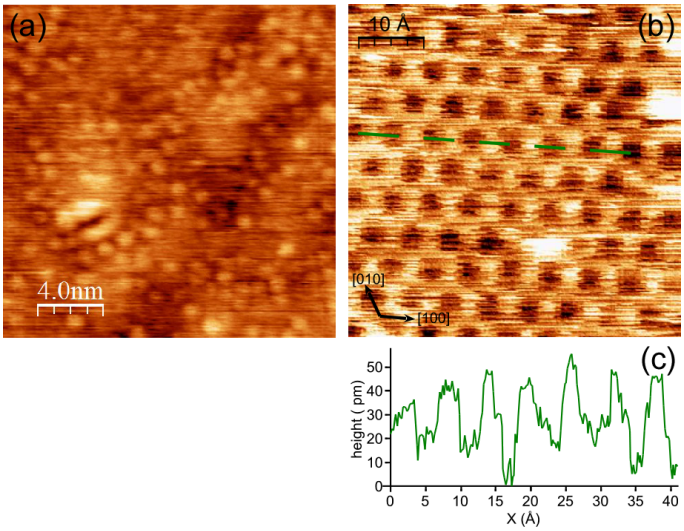

FIG. 2. NC-AFM topography image of AlN(0001) surface after growth of 200 nm thick sample at $T_{\text{substrate}} = 950°C$, $BEP_{NH_3} = 10^{-5}$ Torr and a growth rate of 100 nm/h (a) and 5 nm thick at 10 nm/h (b). (c) Cross section along the dashed line in (b). NC-AFM parameters: (a) $A = 5$ nm, $\Delta f = -65$ Hz, $f_0 = 278.4$ kHz, $Q = 35255$, $U_{\text{sample}} = -4.7$ V; (b)$A = 8$ nm, $\Delta f = -25$ Hz, $f_0 = 274.8$ kHz, $Q = 42780$, $U_{\text{sample}} = -1$ V.

During the growth of the AlN(0001) sample at 100 nm/h, the RHEED measurement exhibits a clear (1×1) pattern indicating that the surface is not reconstructed or highly disordered. This is confirmed by the NC-AFM topography image presented in Fig. 2(a). Despite the observation of fixed features (bright spots) in the image that should correspond to individual atoms, it is not possible to see an apparent periodicity on this surface, whatever the probed area. The disorder observed on this surface can have two origins: 1) the surface is not at equilibrium due to kinetic effects, or 2) the surface is at equilibrium but composed of various reconstructed cells. We will focus in this paper on the second case since the first one is less likely due to a low growth rate compared with the standard one in MBE close to 1 μm/h.

When the growth rate is now reduced to 10 nm/h, the RHEED pattern shows a two-fold symmetry in the <100> and <210> directions indicating the presence of a (2×2) reconstruction. This is confirmed by the NC-AFM topography image in Fig. 2(b). The cross section along the dashed line shows a corrugation of 20 to 30 pm with a noise around 5 pm. The measured periodicity is 6 ± 0.5 Å close to the value $2 \times a_{\text{AlN}} = 6.22$ Å.

To discriminate the reconstruction we are dealing with in Fig. 2-(b), we calculated the Gibbs free energy of formation ΔG^f for the three reconstructions IV(N_{ad}-H+Al-H), V(3Al-H) and VI(N_{ad}) taking the experimental val-

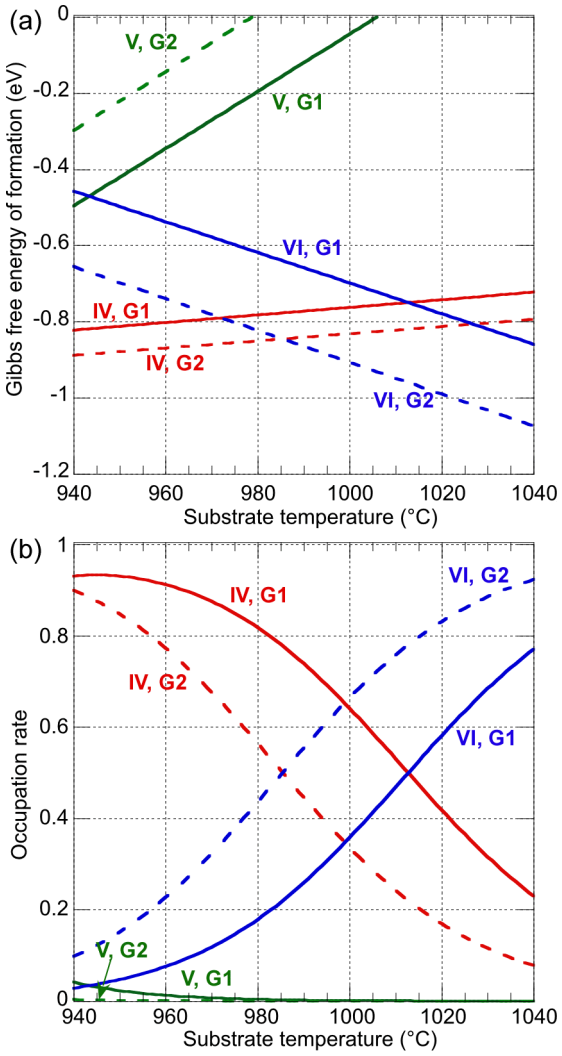

FIG. 3. (a) Gibbs free energy of formation vs substrate temperature for the three reconstructions IV(N_{ad}-H+Al-H), V(3Al-H), and VI(N_{ad}) calculated with the experimental pressures $p_{NH_3} = 2 \times 10^{-6}$ Torr and $p_{Al} = 3 \times 10^{-8}$ Torr, and 3×10^{-9} Torr corresponding to the growth rate G1 and G2 respectively. (b) Occupation rate calculated with the Boltzmann distribution for the three reconstructions and the two sets of growth G1 and G2.

ues for the growth conditions G1 ($p_{Al} = 3 \times 10^{-8}$ Torr, $p_{NH_3} = 2 \times 10^{-6}$ Torr) and G2 ($p_{Al} = 3 \times 10^{-9}$ Torr, $p_{NH_3} = 2 \times 10^{-6}$ Torr) [33]. Figure 3(a) shows the evolution of ΔG^f as a function of the substrate temperature from 940°C to 1040°C. This range corresponds to the experimental temperature window of 960°C-1020°C extended by ±20°C to reflect the 0.1 eV error bar of the DFT calculations [33]. One transition is predicted for each of the two growth conditions: from reconstruction IV to VI at 1013°C for G1, and at 985°C for G2. However, the substrate is at finite temperature and the surface is at its thermodynamic equilibrium where the concentration c_i of a reconstruction i is $c_i = Z_i/Z$, $i \in \mathcal{A}$, with Z the partition function and $\mathcal{A}$ covers all the possible surface reconstructions [45]. The partition function is:

$$Z = \sum_i Z_i = \sum_i g_i \exp\left(\frac{-\Delta G^f}{k_B T_{\text{substrate}}}\right) , \qquad (2)$$

where k_B is the Boltzmann constant and g_i is the degeneracy factor depending on the 2D cell size and on the point symmetry of the reconstruction [45]. For AlN(0001), the reconstructions I to VII, which are mainly involved in NH_3 MBE growth, have all the same (2×2) surface cell and the same (p3m1) point group symmetry leading to an identical g_i factor. The concentration is thus:

$$c_i = \frac{\exp(-\Delta G_i^f / k_B T_{\text{substrate}})}{\sum_{j=I}^{VI} \exp(-\Delta G_j^f / k_B T_{\text{substrate}})} . \qquad (3)$$

Figure 3(b) shows the evolution of the concentration c_i for the three reconstructions and the two growth conditions G1 and G2 over the 940°C–1040°C substrate temperature range. The high temperature leads to a high Boltzmann energy $k_B T_{\text{substrate}} = 0.11$ eV at 1000°C, which tends to create, around the temperature of transition between two reconstructions, a surface formed by a mixture of reconstructed cells of different types.

The NC-AFM observations show a disordered surface for G1 growth conditions and a (2×2) pattern with the presence of a few defects for G2. Looking at Fig. 3(b), the only change between disordered surface and well-ordered surface is obtained for substrate temperature between 1020°C and 1040°C: In this case the surface obtained with G1 growth conditions is formed by a mixture of reconstructed cells of types IV(N_{ad}-H+Al-H) and VI(N_{ad}), while for G2 growth conditions, the surface is mainly (more than 80%) composed by the reconstructed cells of type VI(N_{ad}). This analysis is rather unsensitive to the p_{Al} and p_{NH_3} pressures as shown on the two graphs calculated for $p_{Al} = 3 \times 10^{-8}$ and 3×10^{-9} Torr, $p_{NH_3} = 1 \times 10^{-5}$ Torr and $p_{Al} = 10^{-7}$ and 10^{-8} Torr, $p_{NH_3} = 2 \times 10^{-6}$ Torr [33].

To highlight the effect of temperature, we have plotted in Fig. 4 the iso-concentration curves c_i for three values (0.5, 0.7, and 0.9) on a phase diagram depending on the chemical potentials μ_H and μ_{Al}. The 0.5 iso-concentration curves in between two reconstructed domains follow the usual transition lines drawn on phase diagram. But around the point ($\mu_{Al} = -0.5$ eV, $\mu_H = -1.2$ eV) the 0.5 curves are separated meaning that the surface is mixed with more than two reconstructions. For the 0.7 and 0.9 iso-concentrations curves, the surface is mixed with 0.7 and 0.9 of the main reconstruction and the rest with other reconstructions with a predominance for the closest in ΔG^f energy. For instance, if we consider the point ($\mu_{Al} = -1.5$ eV,$\mu_H = -1.1$ eV), the surface is 90 % of type IV and 10 % of a mixture of other reconstructions with a majority of type VI.

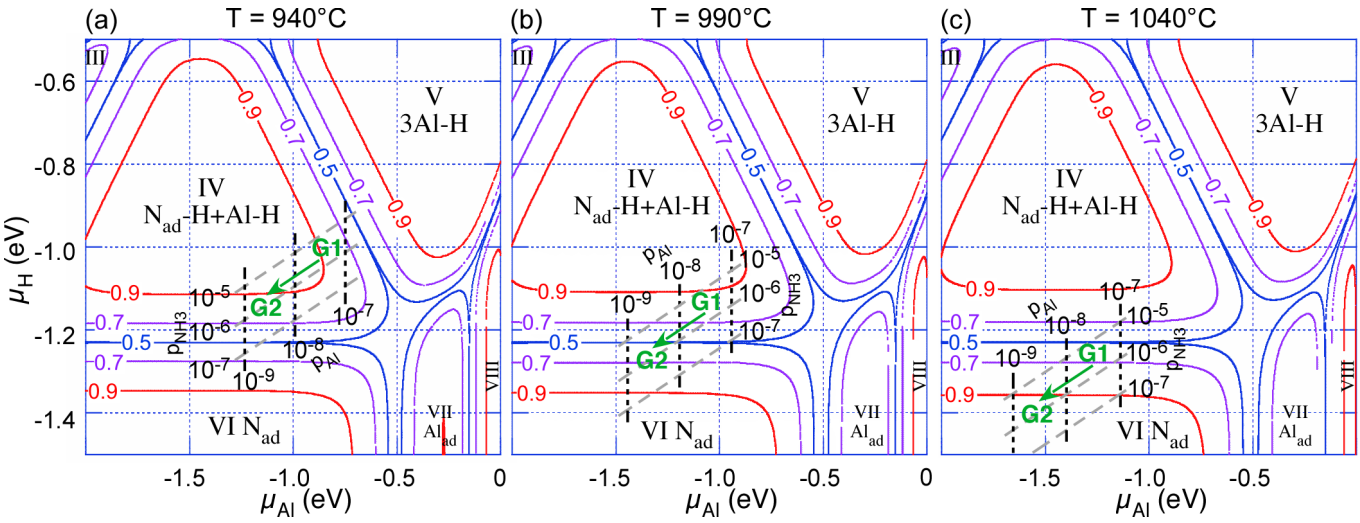

FIG. 4. Phase diagrams with changing temperature: (a) 940°C, (b) 990°C and (c) 1040°C. The iso-concentration curves are blue, purple and red for c_i=0.5, 0.7, and 0.9 respectively. The chemical potentials ($\mu_{\rm Al}, \mu_{\rm H}$) are plotted for three iso-pressures of $p_{\rm Al}$ (black dotted line) and $p_{\rm NH_3}$ (grey dashed line). The beginning and the end of the green arrows indicate the change in chemical potential when passing from G1 to G2 growth conditions.

The effect of the 100°C range on the positionning of these iso-concentration curves is not so important, while it is tremendeous for the chemical potential values calculated for different values of $p_{\rm Al}$ and $p_{\rm NH_3}$. Nevertheless, the same analysis as in Fig. 3(b) can be done for the change between disordered and well-ordered surface observed for the growth conditions G1 and G2. At 940°C the two points are close to the 0.9 iso-concentration curves meaning that the surface should be covered at 90 % with the reconstruction IV in both cases. By increasing the temperature up to 990°C the point G1 is close to the 0.7 curve while G2 is close to the 0.5 one: the disorder is increased between G1 and G2 which is in contradiction with the NC-AFM observations. And finally at 1040°C, G1 is close to the 0.7 curve and G2 to the 0.9 one, leading to a better organization of the surface as observed experimentally.

The high substrate temperature determined theoretically to observe the change between disordered and well-ordered surface means that either the substrate temperature is underestimated or that the chemical potential of NH_3, Al and H species are overestimated. Nevertheless, the analysis of these theoretical results calculated from the experimental error measurements and the theoretical error of 0.1 eV suggests that a transition between a mixed surface and a well-ordered surface mainly of VI(N_{ad}) type is possible.

In summary, we have calculated the phase diagram of the AlN(0001) reconstructed surface in thermodynamic contact with the Al and NH_3 gazeous environment. This approach gives an access to the atomic structure and phase transitions between reconstructed surfaces under realistic MBE growth conditions. In particular, based on DFT calculations, a Bader analysis of the charge distribution of the (2×2) VI(N_{ad}) surface shows that the *electrostatic stability condition* is fulfilled with a surface charge density of $-\sigma/4$ reached at the second bilayer from the surface. This observation could be extended to all the polar semiconductor surfaces with wurtzite or zinc blende structure. Additionally, the use of the Boltzmann distribution accounting for the thermodynamic equilibrium between the reconstructions accessible within our growth conditions suggests that there is a possible transition between a disordered surface obtained at a growth rate of 100 nm/h and a well-ordered surface mainly of (2×2) type VI(N_{ad}) reconstructed when the growth rate is decreased to 10 nm/h. This reconstructed surface with one supplementary N atom per (2×2) cell linked to three aluminum atoms, could be very interesting as a new, more efficient way for doping AlN layer. Indeed Al and N atoms are not saturated during this specific growth by H atoms and thus would be more reactive to bond themselves to other metallic atoms. This opens new routes for the use of AlN in future electronic devices because N-rich AlN surfaces are of fundamental and technological interest due to the high reactivity and in the unprecedent perspective to obtain n- and mostly p-doped AlN material.

The authors thanksfully acknowledge S. Vézian, F. Semond, B. Damilano, Y. Cordier and J. Massies from the CRHEA for their great help in transmitting to us their AlN growth protocol. We also thank M. Portail for the SiC H_2 gas etching and engineers from the AIME for cutting Si and SiC wafers. This work is supported by the European Commission within the projects AtMol (contract N° ICT-270028) and PAMS (contract N° ICT-610446).

Part of the calculation was performed using High Performance Computing resources from the Calcul in Midi-Pyrénées (CALMIP) facilities (grant 2011-[P0832]).

* Permanent address: Centro de Física de Materiales CFM/MPC (CSIC-UPV/EHU), Paseo Manuel de Lardizabal 5, 20018 Donostia-San Sebastián, Spain, and Donostia International Physics Center (DIPC), Paseo Manuel de Lardizabal 4, 20018 Donostia-San Sebastián, Spain

† david.martrou@cemes.fr

[1] B. S. Eller, J. Yang, and R. J. Nemanich, J. Vac. Sci. Technol. A **31**, 050807 (2013).
[2] J. Li, K. B. Nam, M. L. Nakarmi, J. Y. Lin, H. X. Jiang, P. Carrier, and S.-H. Wei, Appl. Phys. Lett. **83**, 5163 (2003).
[3] O. Ambacher, J. Phys. D: Appl. Phys. **31**, 2653 (1998).
[4] J. R. Mileham, S. J. Pearton, C. R. Abernathy, J. D. MacKenzie, R. J. Shul, and S. P. Kilcoyne, J. Vac. Sci. Technol. A **14**, 836 (1995).
[5] G. Li, B. Song, S. Ganguly, M. Zhu, R. Wang, X. Yan, J. Verma, V. Protasenko, H. Grace Xing, and D. Jena, Appl. Phys. Lett. **104**, 193506 (2014).
[6] J. E. Northrup, R. Di Felice, and J. Neugebauer, Phys. Rev. B **55**, 13878 (1997).
[7] H. Suzuki, R. Togashi, H. Murakami, Y. Kumagai, and A. Koukitu, Jpn. J. Appl. Phys. **46**, 5112 (2007).
[8] M. S. Miao, A. Janotti, and C. G. Van de Walle, Phys. Rev. B **80**, 155319 (2009).
[9] T. Akiyama, T. Yamashita, K. Nakamura, and T. Ito, J. Cryst. Growth **318**, 79 (2011).
[10] T. Akiyama, D. Obara, K. Nakamura, and T. Ito, Jpn. J. Appl. Phys. **51**, 018001 (2012).
[11] H. Şahin, S. Cahangirov, M. Topsakal, E. Bekaroglu, E. Akturk, R. T. Senger, and S. Ciraci, Phys. Rev. B **80**, 155453 (2009).
[12] P. W. Tasker, J. Phys. C: Solid State Phys. **12**, 4977 (1979).
[13] C. Noguera, J. Phys.: Condens. Matter **12**, R367 (2000).
[14] C. D. Lee, Y. Dong, R. M. Feenstra, J. E. Northrup, and J. Neugebauer, Phys. Rev. B **68**, 205317 (2003).
[15] T. R. Albrecht, P. Grütter, D. Horne, and D. Rugar, J. Appl. Phys. **69**, 668 (1991).
[16] A. S. Foster, C. Barth, A. L. Shluger, and M. Reichling, Phys. Rev. Lett. **86**, 2373 (2001).
[17] M. A. Venegas de la Cerda, J. Abad, A. Madgavkar, D. Martrou, and S. Gauthier, Nanotechnology **19**, 045503 (2008).
[18] B. Such, T. Glatzel, S. Kawai, S. Koch, and E. Meyer, J. Vac. Sci. Technol. B **28**, C4B1 (2010).
[19] C. Barth and C. R. Henry, Phys. Rev. Lett. **91**, 196102 (2003).
[20] C. Barth and M. Reichling, Nature (London) **414**, 54 (2001).
[21] K.-i. Fukui, Y. Namai, and Y. Iwasawa, Appl. Surf. Sci. **188**, 252 (2002).
[22] K.-i. Fukui, H. Onishi, and Y. Iwasawa, Phys. Rev. Lett. **79**, 4202 (1997).
[23] J. V. Lauritsen and M. Reichling, J. Phys.: Condens. Matter **22**, 263001 (2010).
[24] M. K. Rasmussen, A. S. Foster, F. F. Canova, B. Hinnemann, S. Helveg, K. Meinander, F. Besenbacher, and J. V. Lauritsen, Phys. Rev. B **84**, 235419 (2011).
[25] P. Rahe, J. Schütte, and A. Kühnle, J. Phys.: Condens. Matter **24**, 084006 (2012).
[26] F. J. Giessibl, Science **267**, 68 (1995).
[27] J. J. Kolodziej, B. Such, and M. Szymonski, Phys. Rev. B **71**, 165419 (2005).
[28] J. J. Kolodziej, B. Such, M. Szymonski, and F. Krok, Phys. Rev. Lett. **90**, 226101 (2003).
[29] M. Nimmrich, M. Kittelmann, P. Rahe, A. J. Mayne, G. Dujardin, A. von Schmidsfeld, M. Reichling, W. Harneit, and A. Kühnle, Phys. Rev. B **81**, 201403(R) (2010).
[30] D. Martrou, L. Guiraud, R. Laloo, B. Pecassou, P. Abeilhou, O. Guillermet, E. Dujardin, S. Gauthier, J. Polesel Maris, M. Venegas, A. Hinault, A. Bodin, F. Chaumeton, A. Piednoir, H. Guo, and T. Leoni, in *Atomic Scale Interconnection Machines*, edited by C. Joachim (Springer Berlin Heidelberg, 2012) pp. 35–52.
[31] I. Vurgaftman and J. R. Meyer, J. Appl. Phys. **94**, 3675 (2003).
[32] J. Goniakowski, F. Finocchi, and C. Noguera, Rep. Prog. Phys. **71**, 016501 (2008).
[33] See Supplemental Material at [URL will be inserted by publisher] for details on DFT calculations, Bader charges tables, substrate temperature measurement and the additionnal $\Delta G_i^f = f(T_{substrate})$ graphs.
[34] G. Henkelman, A. Arnaldsson, and H. Jónsson, Comput. Mater. Sci. **36**, 354 (2006).
[35] C. G. Van de Walle and J. Neugebauer, J. Vac. Sci. Technol. B **20**, 1640 (2002).
[36] G. Kresse and J. Furthmüller, Comput. Mater. Sci. **6**, 15 (1996).
[37] G. Kresse and J. Furthmüller, Phys. Rev. B **54**, 11169 (1996).
[38] G. Kresse and D. Joubert, Phys. Rev. B **59**, 1758 (1999).
[39] P. E. Blöchl, Phys. Rev. B **50**, 17953 (1994).
[40] J. P. Perdew, K. Burke, and M. Ernzerhof, Phys. Rev. Lett. **77**, 3865 (1996).
[41] K. Shiraishi, J. Phys. Soc. Jpn **59**, 3455 (1990).
[42] J. Li and L.-W. Wang, Phys. Rev. B **72**, 125325 (2005).
[43] Y. Kangawa, T. Ito, A. Taguchi, K. Shiraishi, and T. Ohachi, Surf. Sci. **493**, 178 (2001).
[44] F. Chaumeton, S. Gauthier, and D. Martrou, AIP Adv. **5**, 067108 (2015).
[45] O. Romanyuk, F. Grosse, A. Proessdorf, W. Braun, and H. Riechert, Physical Review B **82** 125315 (2010)
.